



Contents lists available at ScienceDirect

Journal of Alloys and Compounds

journal homepage: www.elsevier.com/locate/jalcom

Intermetallic phases in Mg–Co–Y alloys

Qian-Qian Jin^a, Shao-Bo Mi^{a,b,*}^aShenyang National Laboratory for Materials Science, Institute of Metal Research, Chinese Academy of Sciences, Shenyang 110016, People's Republic of China^bInternational Center for Dielectric Research (ICDR), Xi'an Jiaotong University, Xi'an 710049, People's Republic of China

ARTICLE INFO

Article history:

Received 21 May 2013

Received in revised form 6 July 2013

Accepted 7 August 2013

Available online 17 August 2013

Keywords:

Magnesium alloys

Crystal structure

Intermetallics

Electron microscopy

ABSTRACT

The microstructural details and phase evolution of the as-cast and annealed Mg₈₈Co₅Y₇(at.%) alloys were characterized by means of electron microscopies. Two new crystalline phases were revealed in the Mg–Co–Y alloys. They are hexagonal with composition of about Mg_{70–73}Co₅Y_{22–25} (Mg₃(Co,Y)) ($a = 1.04$ nm, $c = 2.25$ nm, $P6_3/mmc$) and face-centered cubic with a composition of about Mg₁₅Y₂₁Co₆₄ (MgYCo₄) ($a = 0.707$ nm, $F43m$), isostructural to MgSnCu₄. In addition, a new crystallographic orientation relationship between Mg and Mg₂₄Y₅ has been observed.

© 2013 Elsevier B.V. All rights reserved.

1. Introduction

Intermetallic magnesium compounds play a very important role in precipitation hardening [1–3] in lightweight structural materials and in hydrogen storage applications [4–6], which stimulates the intensive study of structure, crystal chemistry and mechanical properties in the ternary alloys of magnesium (Mg)–transition metal (TM)–rare earth metal (RE) [7–10]. Recently, Inoue et al. reported that mechanical properties of magnesium-based alloys Mg₉₇Y₂Zn₁ (at.%) with long period stacking ordered (LPSO) structures exhibit significant improvement both at room temperature and elevated temperatures [11]. Detailed structure investigations indicated the formation of four types of LPSO structures (10H, 14H, 18R and 24R) in the Mg–Zn–Y alloys [12–14]. More recently, new polytypes of LPSO structures of 15R, 12H and 21R was observed in as-cast Mg–Co–Y alloys. In contrast to the LPSO structures in Mg–Zn–Y alloys, the new polytypes of LPSO structures consist of a structural unit of AB'C-type trilateral stacking in the stacking sequence of the close-packed atomic layers [15]. Nevertheless, the microstructural details and phase evolution (e.g. LPSO structures) in the Mg–Co–Y alloys upon annealing were still not established.

In the present work, we studied the microstructural properties of the Mg₈₈Co₅Y₇ alloys by means of scanning electron microscopy (SEM), transmission electron microscopy (TEM) and scanning transmission electron microscopy (STEM). Phase evolution of LPSO structures in the course of heat treatment was established. In addition,

two phases of Mg₃(Co,Y) and MgYCo₄ were identified as a hexagonal and a face-centered cubic, respectively. In the annealed Mg₈₈Co₅Y₇ alloys, a new orientation relationship between Mg and Mg₂₄Y₅(β) was determined, $(0001)_{Mg} // (\bar{1}10)_{\beta}$ and $[11\bar{2}0]_{Mg} // [110]_{\beta}$.

2. Experimental procedures

A ternary alloy with a nominal composition Mg₈₈Co₅Y₇(at.%) was prepared by melting the high purity pure Mg, Co and Mg–30 wt.%Y master alloys in a graphite crucible under protection of ultrahigh purity argon atmosphere in a high frequency induction melting furnace, and then cooled down to the room temperature under the argon atmosphere in the furnace. Several small pieces were cut from the as-cast ingot, and sealed in quartz tube filled with argon, then annealed at 673 K for 16 h and at 773 K for 10 h, respectively, followed by water quenching.

The microstructural properties of the samples were examined by SEM, TEM and STEM. The volume fraction of phases on SEM images was evaluated by image analysis software (SISC-IAS). Selected area electron diffraction (SAED) patterns were recorded in a JEOL JEM2100 microscope. The local chemical composition was measured in a scanning electron microscope and a Tecnai G² F30 microscope equipped with an energy-dispersive X-ray (EDX) detector. Atomic resolution high-angle annular dark field (HAADF) images were obtained in a JEM ARM200F microscope equipped with a probe corrector, operated at 200 kV. The probe convergence semi-angle was 25 mrad and the inner collection angle of the HAADF detector was 90 mrad. Thin foils for TEM and STEM observations were prepared by grinding, polishing, dimpling and Ar ion milling.

* Corresponding author at: Shenyang National Laboratory for Materials Science, Institute of Metal Research, Chinese Academy of Sciences, Shenyang 110016, People's Republic of China. Tel.: +86 24 23971843; fax: +86 24 23891320.

E-mail address: sbmi@imr.ac.cn (S.-B. Mi).

3. Results and discussion

3.1. Microstructure and morphology evolution of $Mg_{88}Co_5Y_7$ alloy during heat treatment

Fig. 1a–c shows back-scattered electron (BSE) SEM images of the as-cast alloy, the alloys annealed at 673 K for 16 h and at 773 K for 10 h, respectively. Under the BSE-SEM imaging conditions, the phases with different compositions can be imaged as different (greyscale) contrast. In Fig. 1a–c, a phase with chemical composition of $Mg_{15}Y_{21}Co_{64}$ shows the brightest contrast. We refer this phase as $MgYCo_4$. A phase shows brighter contrast with chemical composition of $Mg_{70-73}Co_5Y_{22-25}$, namely, $Mg_3(Co,Y)$. $Mg_{24}Y_5$ phase presents bright contrast, LPSO grey contrast and the Mg matrix dark contrast. In the as-cast samples shown in Fig. 1a, the volume fraction of Mg, LPSO, $Mg_3(Co,Y)$ and $Mg_{24}Y_5$ is about 65.1%, 27.7%, 4.3% and 0.9%, respectively. $MgYCo_4$ phase appears within the Mg matrix and its volume fraction is about 2.0%.

After annealing at 673 K for 16 h, the volume fraction of $MgYCo_4$ and $Mg_{24}Y_5$ increases to about 3.2% and 8.2%, respectively. In

contrast, the volume fraction of $Mg_3(Co,Y)$ decreases to about 1.5%. For $Mg_{24}Y_5$ phase, two types of morphology of either irregular or plate-like appear after annealing. The $Mg_{24}Y_5$ phase with plate-like morphology distributes mainly in the LPSO. The solubility of Y in the Mg matrix decreases from 3.4% in the as-cast samples to 2.0% in the annealed samples at 673 K.

After annealing at 773 K for 10 h, the volume fraction of $Mg_{24}Y_5$ phase with irregular morphology increases to about 11.4% and $Mg_{24}Y_5$ phase with plate-like morphology disappears. The volume fraction of $MgYCo_4$ phase is about 3.4% and $Mg_3(Co,Y)$ phase is completely melted at this temperature. The LPSO structures with very small amount still exist at this temperature. The solubility of Co in $Mg_{24}Y_5$ and Mg is very limited, which seems independent of heat treatment. It is necessary to mention that the annealing duration is quite short for our samples to avoid some serious oxidation problems. As a consequence, the phase equilibrium in the annealed samples was not completely obtained, e.g. the existence of more than three phases in Fig. 1b and c.

3.2. Intermetallic phases

3.2.1. LPSO

15R-, 12H-, 21R- and 18R-typed LPSO structures were observed in the as-cast $Mg_{88}Co_5Y_7$ alloy [15]. After annealing at 673 K for 16 h, these four types of LPSO structures still exist in the annealed alloy and the 15R- and 12H-typed LPSO structures are in the majority confirmed by TEM observations. Nevertheless, after annealing at 773 K for 10 h, only 18R-typed LPSO structure remains. Our HAADF-STEM investigation indicates that for the 15R-, 12H-, 21R- and 18R-typed LPSO structures there is no structural difference between the as-cast and the annealed alloys.

3.2.2. $Mg_3(Co,Y)$

Fig. 2a shows a low-magnification TEM image of the as-cast $Mg_{88}Co_5Y_7$ alloy. $Mg_3(Co,Y)$ phase with dark contrast adjoins LPSO and $Mg_{24}Y_5$ distributed in the Mg matrix, which consists to the microstructure in Fig. 1a. The chemical composition of $Mg_3(Co,Y)$ phase is in a range of $Mg_{70}Co_5Y_{25}$ – $Mg_{73}Co_5Y_{22}$ measured by EDX in TEM mode. We noted that the chemical composition of $Mg_3(Co,Y)$ phase is affected by its neighboring phases. $Mg_3(Co,Y)$ phase adjacent to the Mg matrix has higher Mg content and adjacent to the $Mg_{24}Y_5$ has higher Y content. The interdiffusion between $Mg_3(Co,Y)$ phase and its neighboring phases may occur during the heat treatment of the alloys. The SAED patterns of main zone axis of $Mg_3(Co,Y)$ were shown in Fig. 2b–d, respectively. The diffraction spots in the SAED pattern in Fig. 2b exhibit a three- or sixfold symmetry. The SAED pattern in Fig. 2c was obtained from Fig. 2d by large-angle tilting experiments and the tilted angle between Fig. 2c and Fig. 2d is 30°. Fig. 2c and Fig. 2d could not be indexed satisfactorily in a cubic structure. Assuming that $Mg_3(Co,Y)$ phase is a hexagonal, Fig. 2b–d can be well indexed as [0001], [11 $\bar{2}$ 0] and [1 $\bar{1}$ 00] zone axis, respectively. The lattice parameters of $Mg_3(Co,Y)$ phase are $a = 1.04$ nm and $c = 2.25$ nm, calculated from the SAED patterns.

In Fig. 2c, the 000 l spots with $l = \text{odd}$ are rather weak but still discernible, indicated by a pair of horizontal arrows. Fig. 2e shows a typical high-resolution HAADF image of $Mg_3(Co,Y)$ phase, recorded along its [11 $\bar{2}$ 0] zone axis. The insert in Fig. 2e is the fast Fourier transform (FFT) pattern of the HAADF image of $Mg_3(Co,Y)$ phase. It is clearly that the 000 l spots with $l = \text{odd}$ in the FFT pattern are extinctions, which indicates that a 6 $_3$ screw axis is parallel to [0001] zone axis and weak contrast of the 000 l spots with $l = \text{odd}$ showing in Fig. 2c results from the double diffraction.

Based on the SAED patterns in Fig. 2b–d, the reflection conditions for the occurrence of diffraction spots are summarized as follows: 000 l : $l = 2n$; $hh\bar{2}hl$: $l = 2n$ and $hh0l$: $l = \text{integer}$. Thus, the

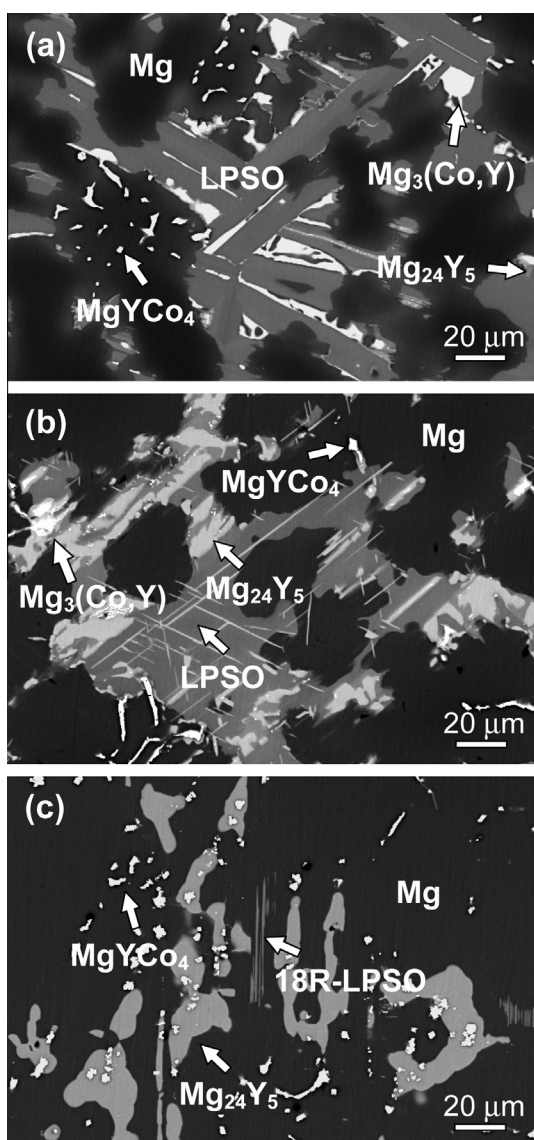


Fig. 1. Back-scattered electron (BSE) images of the $Mg_{88}Co_5Y_7$ alloy: (a) as-cast, (b) annealed at 673 K for 16 h and (c) annealed at 773 K for 10 h, respectively. The Mg matrix shows dark contrast, the LPSO light grey contrast, the $Mg_{24}Y_5$ phase grey contrast, the $Mg_3(Co,Y)$ brighter contrast and the $MgYCo_4$ the brightest contrast.

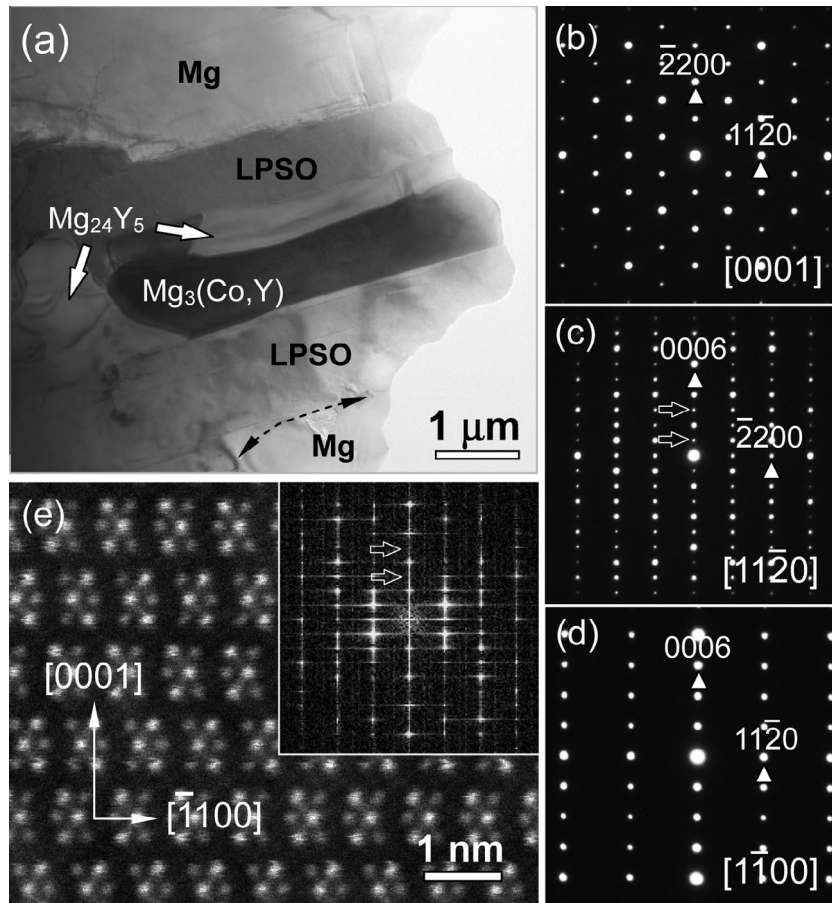


Fig. 2. (a) A low-magnification TEM image of the as-cast $\text{Mg}_{88}\text{Co}_5\text{Y}_7$ alloy, showing the coexistence of $\text{Mg}_3(\text{Co,Y})$ with LPSO structures, Mg_{24}Y_5 and Mg. SAED patterns of the $\text{Mg}_3(\text{Co,Y})$ phase taken with the incident beam parallel to (b) $[0001]$, (c) $[11\bar{2}0]$ and (d) $[1\bar{1}00]$ zone axis, respectively. (e) An atomic-resolution HAADF image of $\text{Mg}_3(\text{Co,Y})$ phase, recorded along $[11\bar{2}0]$ zone axis. The insert is its FFT pattern showing the extinctions of $000l$ spots with $l = \text{odd}$.

Table 1
Diffraction group(s) and whole pattern (WP) symmetry of the possible point groups.

Point group	$[0001]$		$[UV.0]$	
	Diffraction group	WP symmetry	Diffraction group	WP symmetry
$6/mmm$	$6mm1_R$	$6mm$	2_Rmm_R	m
$6m2$	$3m1_R$	$3m$	m	m
$6mm$	$6mm$	$6mm$	m_R	1

possible space group is $P6_3mc$, $P6_2c$ and $P6_3/mmc$, which belongs to point group of $6mm$, $6m2$ ($62m$) and $6/mmm$, respectively [16]. According to the diffraction group and whole pattern of $6/mmm$, $6m2$ ($62m$) and $6mm$ from $[0001]$ and $[UV.0]$ shown in Table 1, the point group of $\text{Mg}_3(\text{Co,Y})$ phase can be determined by obtaining the whole pattern from $[0001]$ and $[UV.0]$ zone axis, respectively.

To further determine the point group of $\text{Mg}_3(\text{Co,Y})$ phase, a microanalytical technique of convergent beam electron diffraction (CBED) was performed on our samples. Fig. 3a and b are the CBED patterns obtained from small specimen regions by a convergent beam of electrons along $[0001]$ zone axis and $[UV.0]$ zone axis (slight away from $[11\bar{2}0]$ zone axis), respectively. The analysis of the symmetry in Fig. 3a reveals that $\text{Mg}_3(\text{Co,Y})$ phase has a sixfold rotational symmetry and two independent mirror planes of M1 and M2. It means that the whole pattern symmetry of $\text{Mg}_3(\text{Co,Y})$ has $6mm$ symmetry along $[0001]$ zone axis. Fig. 3b shows the

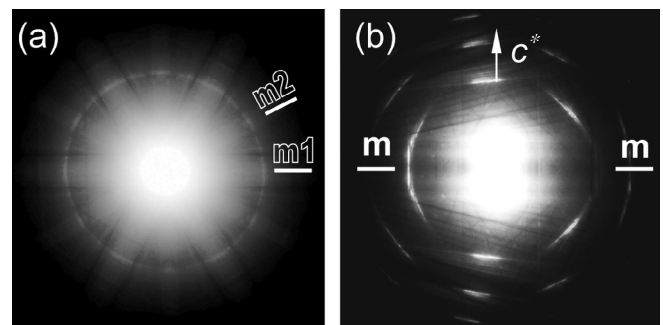


Fig. 3. CBED patterns of $\text{Mg}_3(\text{Co,Y})$ taken along (a) $[0001]$ and (b) $[UV.0]$ zone axis slight away from $[11\bar{2}0]$ zone axis, respectively. The whole pattern in (a) shows not only a sixfold rotational symmetry but also two independent mirror planes ($m1$ and $m2$), in (b) shows a mirror plane perpendicular to $[0001]$ direction.

whole pattern of $\text{Mg}_3(\text{Co,Y})$ obtained from $[UV.0]$ zone axis, indicating a mirror plane perpendicular to $[0001]$ direction. Therefore, according to the data in Table 1, the point group can be derived as $6/mmm$ and the space group as $P6_3/mmc$ for $\text{Mg}_3(\text{Co,Y})$ phase. It is noted that no binary phase related to the $\text{Mg}_3(\text{Co,Y})$ phase was reported in the system of Mg–Co and Mg–Y. No apparent orientation relationship between $\text{Mg}_3(\text{Co,Y})$ phase with other intermetallic phases was observed in our work.

3.2.3. MgYCo_4

Recently, a ternary phase of CoMgY_4 was reported in the Mg–Co–Y system, which is isomorphous with the Gd_4RhIn structure

(space group $F\bar{4}3m$) [17]. This phase was not found in our samples in the course of SEM/TEM observations. Instead, a ternary phase of MgYCo_4 with chemical composition of about $\text{Mg}_{15}\text{Y}_{21}\text{Co}_{64}$ was observed.

Fig. 4a is a low-magnification TEM image showing the coexistence of MgYCo_4 phase with Mg. No orientation relationship between these two phases was detected. In some cases, the contrast variation in MgYCo_4 grains was visible, which comes from the existence of planar defects (e.g. twin) in the crystal. A representative EDX spectrum recorded from the MgYCo_4 phase was shown in Fig. 4b. The SAED patterns of the main zone axis of MgYCo_4 were presented in Fig. 4c–e, obtained by large-angle tilting experiments in TEM, which can be indexed as zone axis of [100], [110] and [111] of a face-centered cubic, respectively. The lattice parameter of MgYCo_4 phase was measured to be $a = 0.707$ nm.

It is known that in the Mg–Ni–Y systems, a ternary phase of MgYNi_4 ($a = 0.71853$ nm) isomorphous with MgSnCu_4 was reported (space group $F\bar{4}3m$) [18]. MgYCo_4 phase might also be isomorphous with the MgSnCu_4 structure.

3.3. Orientation relationship between $\text{Mg}_{24}\text{Y}_5(\beta)$ and Mg

$\text{Mg}_{24}\text{Y}_5(\beta)$ has a body-centered cubic structure with lattice parameter of $a = 1.1204$ nm [19]. In the Mg–Y system, an orientation relationship between β and Mg have been determined, $(0001)_{\text{Mg}}//(\bar{0}11)_{\beta}$ and $[11\bar{2}0]_{\text{Mg}}//[1\bar{1}1]_{\beta}$ [20], which is also the overwhelming majority of orientation relationship between β and Mg in the Mg–Co–Y system.

In addition, another type of orientation relationship between β and Mg was observed in our TEM observations. Fig. 5a is a

low-magnification TEM image showing that β phase adjoins with $\text{Mg}_3(\text{Co},\text{Y})$ and Mg. The SAED pattern taken along [11 $\bar{2}$ 0] zone axis of Mg was shown in Fig. 5b, which was obtained by using an aperture covering the β phase and the Mg matrix. Apart from the diffraction spots of Mg, the other diffraction spots in the SAED pattern can be indexed as β phase viewed along its [110] zone axis. Indexing the SAED pattern, an orientation relationship between β and Mg was determined, $(0001)_{\text{Mg}}//(\bar{1}10)_{\beta}$ and $[11\bar{2}0]_{\text{Mg}}//[110]_{\beta}$. It is necessary to mention that this type of orientation relationship between β and Mg was in the minority in our TEM experiments.

A typical high-resolution TEM lattice image of Mg– β interface was shown in Fig. 5c, recorded with the incident beam parallel to the [11 $\bar{2}$ 0]_{Mg} zone axis. The Mg– β interface was indicated by a vertical arrow. It can be seen that the Mg– β interface is atomically sharp, which can be easily recognized due to the different crystal structure between Mg and β . Based on the lattice parameter of Mg ($a = 0.3203$ nm and $c = 0.5197$ nm) [21] and β , for orientation relationship of $(0001)_{\text{Mg}}//(\bar{1}10)_{\beta}$ and $[11\bar{2}0]_{\text{Mg}}//[110]_{\beta}$ between Mg and β , the lattice mismatch between d_{100} (0.2774 nm) for Mg and d_{004} (0.2801 nm) for β is 0.97%, and between d_{002} (0.2599 nm) for Mg and $d_{3\bar{3}0}$ (0.2641 nm) for β is 1.62%, respectively.

In comparison, for the orientation relationship of $(0001)_{\text{Mg}}//(\bar{0}11)_{\beta}$ and $[11\bar{2}0]_{\text{Mg}}//[1\bar{1}1]_{\beta}$ between β and Mg, the lattice match between $d_{11\bar{2}0}$ (0.1602 nm) for Mg and $d_{4\bar{4}4}$ (0.1617) for β is 0.94%, and between d_{002} (0.2598 nm) for Mg and d_{033} (0.2641) for β is 1.66%, respectively. We can see that the lattice match between these two types of orientation relations is comparable, which may be in favor of their coexistence in Mg–Co–Y. Nevertheless, the orientation relationship of $(0001)_{\text{Mg}}//(\bar{0}11)_{\beta}$ and $[11\bar{2}0]_{\text{Mg}}//$

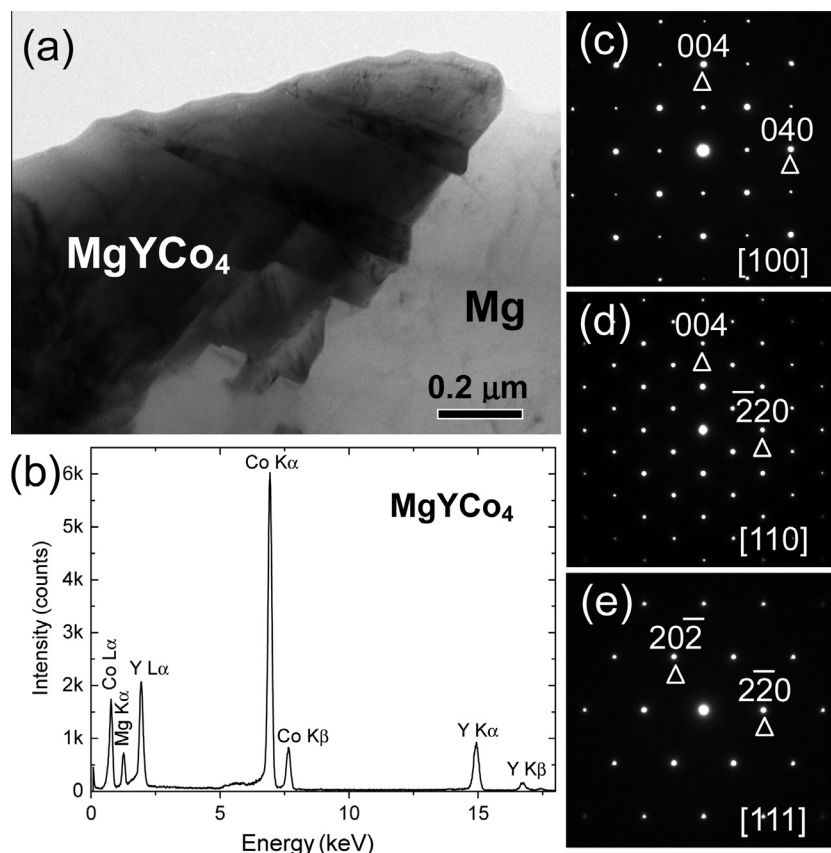


Fig. 4. (a) A low-magnification TEM image of the as-cast $\text{Mg}_{88}\text{Co}_5\text{Y}_7$ alloy, showing the coexistence of MgYCo_4 and Mg. (b) An EDX spectrum recorded from the MgYCo_4 phase. SAED patterns of MgYCo_4 phase, taken with the incident beam parallel to (c) [100], (d) [110] and (e) [111] zone axis, respectively.

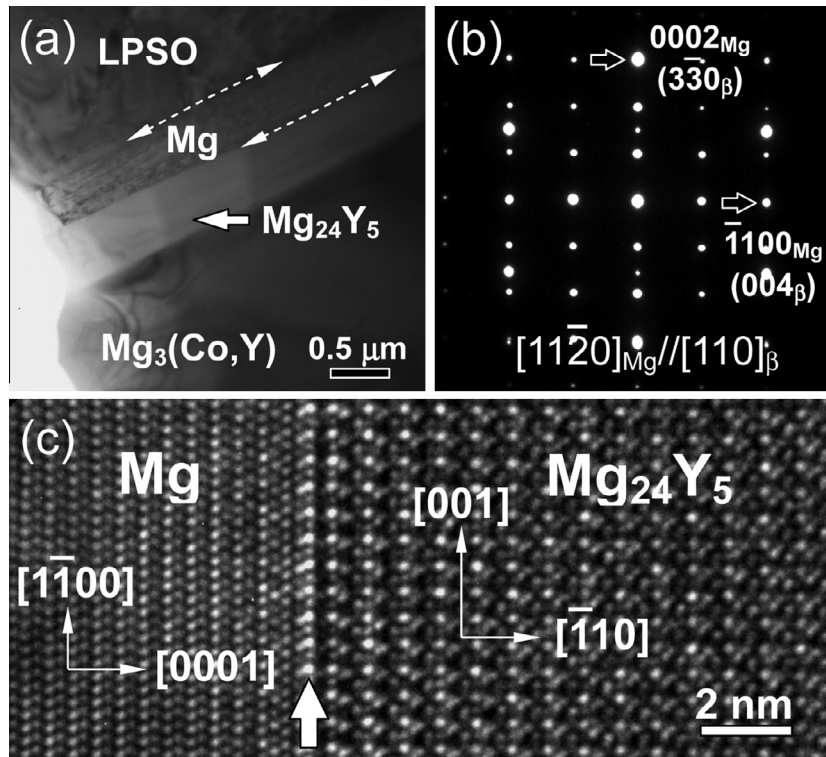


Fig. 5. (a) A low-magnification TEM image of the annealed Mg₈₈Co₅Y₇ alloy, indicating the coexistence of Mg₃(Co,Y), Mg₂₄Y₅(β), LPSO and Mg. (b) An SAED pattern shows the orientation relationship, (0001)_{Mg}//($\bar{1}10$)_β and [1120]_{Mg}//[110]_β, between Mg and Mg₂₄Y₅, taken along [1120]_{Mg} zone axis. (c) A high-resolution TEM lattice image of the Mg–Mg₂₄Y₅ interface. The interface was indicated by a vertical arrow.

$[1\bar{1}1]_{\beta}$ between Mg and β is very great in amount, which implies that apart from the lattice mismatch, other factors, e.g. interface structure, may also affect the stability of orientation relationship in the Mg–Co–Y system.

4. Conclusion

We studied the microstructural properties of the as-cast and annealed Mg₈₈Co₅Y₇(at.%) alloys. Apart from LPSO structures, two intermetallic phases, Mg₃(Co,Y) and MgYCo₄, were observed in the as-cast and annealed alloys. The Mg₃(Co,Y) phase has a hexagonal structure ($a = 1.04$ nm, $c = 2.25$ nm, $P6_3/mmc$) and the MgYCo₄ phase has a face-centered cubic structure ($a = 0.707$ nm). A new orientation relationship between Mg and Mg₂₄Y₅(β) was determined to be (0001)_{Mg}//($\bar{1}10$)_β and [1120]_{Mg}//[110]_β.

Acknowledgements

We are grateful to Prof. H.F. Zhang (Institute of Metal Research, China) for providing access to the sample preparation facilities, and to Prof. C.L. Jia (Xi'an Jiaotong University, China) for fruitful discussions. The work was financially supported by the Ministry of Science & Technology of China (2009CB623705) and the Hundred Talents Project of Chinese Academy of Sciences. The atomic-resolution HAADF investigation of samples was performed on the TEM platform for dielectrics research, Xi'an Jiaotong University, China.

References

- M. Ahmed, G.W. Lorimer, P. Lyon, R. Pillington, *Magnesium Alloys and Their Applications*, in: B.L. Mordike, F. Hehmann (Eds.), Editors, DGM Informationsgesellschaft m.b.H, Alle Rechte vorbehalten, 1992, pp. 301–308.
- N. Hort, Y.D. Huang, K.U. Kainer, *Adv. Eng. Mater.* 8 (2006) 235–240.
- A.A. Luo, *Int. Mater. Rev.* 49 (2004) 13–30.
- M.H. Mintz, Z. Gavra, G. Kimmel, Z. Hadari, *J. Less-Common Met.* 74 (1980) 263–270.
- S. Orimo, H. Fujii, *Intermetallics* 6 (1998) 185–192.
- L. Schlapbach, A. Züttel, *Nature* 414 (2001) 353–358.
- T. Itoi, K. Takahashi, H. Moriyama, M. Hirohashi, *Scripta Mater.* 59 (2008) 1155–1158.
- K. Amiya, T. Ohsuna, A. Inoue, *Mater. Trans.* 44 (2003) 2151–2156.
- K. Kishida, H. Yokobayashi, H. Inui, M. Yamasaki, Y. Kawamura, *Intermetallics* 31 (2012) 55–64.
- Y. Kawamura, T. Kasahara, S. Izumi, M. Yamasaki, *Scripta Mater.* 55 (2006) 453–456.
- A. Inoue, Y. Kawamura, M. Matsushita, K. Hayashi, J. Koike, *J. Mater. Res.* 16 (2001) 1894–1900.
- Y.M. Zhu, A.J. Morton, J.F. Nie, *Acta Mater.* 60 (2012) 6562–6572.
- E. Abe, A. Onoa, T. Itoi, M. Yamasaki, Y. Kawamura, *Philos Mag. Lett.* 91 (2011) 690–696.
- J.E. Saal, C. Wolverton, *Scripta Mater.* 67 (2012) 798–801.
- S.B. Mi, Q.Q. Jin, *Scripta Mater.* 68 (2013) 635–638.
- D.B. Williams, C.B. Carter, *Transmission electron microscopy: A textbook for materials science*, Plenum, New York, 1996, pp. 357–361.
- S. Tuncel, R.D. Hoffmann, B. Chevalier, S.F. Matar, R. Pöttgen, *Z. Anorg. Allg. Chem.* 633 (2007) 151–157.
- K. Kadir, D. Noreus, I. Yamashita, *J. Alloys Comp.* 345 (2002) 140–143.
- E.G. Gibson, O.N. Carlson, *Trans. Am. Soc. Met.* 52 (1960) 1084–1096.
- M.X. Zhang, P.M. Kelly, *Scripta Mater.* 48 (2003) 379–384.
- W.B. Pearson, P. Villars, L.D. Calvert, in: *Pearson's handbook of crystallographic data for intermetallic phases*, ASM, 1985, p. 2336.